



Providing Choice & Value

Generic CT and MRI Contrast Agents



FRESENIUS
KABI

CONTACT REP

AJNR

MR imaging of pituitary adenomas using a prototype resistive magnet: preliminary assessment.

R Oot, P F New, F S Buonanno, I L Pykett, P Kistler, R Delapaz, K R Davis, J M Taveras and T J Brady

This information is current as of July 21, 2025.

AJNR Am J Neuroradiol 1984, 5 (2) 131-137
<http://www.ajnr.org/content/5/2/131>

MR Imaging of Pituitary Adenomas Using a Prototype Resistive Magnet: Preliminary Assessment

Robert Oot¹
 Paul F. J. New¹
 Ferdinando S. Buonanno¹
 Ian L. Pykett²
 Philip Kistler²
 Robert Delapaz¹
 Kenneth R. Davis¹
 Juan M. Taveras¹
 Thomas J. Brady¹

Magnetic resonance (MR) images were obtained with a prototype resistive magnet system in 10 patients, all of whom had been shown to have pituitary tumors by enhanced high-resolution computed tomography (CT). Histologic verification was obtained in eight cases. Inversion-recovery (IR) T1-weighted images revealed the tumor in six of nine cases; saturation-recovery (SR) images with less T1 weighting identified seven of nine tumors; Carr-Purcell-Meiboom-Gill (CPMG) spin-echo T2-weighted images revealed two of four tumors. MR images failed to demonstrate three microadenomas: 5 × 5 × 8 mm, 6 × 6 × 6 mm, and one less than 5 mm in estimated size. In the last pretreatment study, CT had demonstrated a 13 mm maximum diameter adenoma. Repeat CT at the time of MR imaging also showed a partially empty sella and did not resolve the residual adenoma. The larger adenomas were identified readily by MR imaging, which, unlike CT, suggested old tumor hemorrhage in two cases, which was confirmed at surgery and histologic examination. MR and CT images were also compared for relative effectiveness in identifying important perisellar structures.

The introduction of computed tomography (CT) has revolutionized the imaging of intracranial neoplasms. High-resolution CT has been shown to have high sensitivity in detecting pituitary tumors and represents the standard against which any new imaging method must be measured. Previous publications dealing with magnetic resonance (MR) imaging of intracranial lesions have generally included examples of a wide variety of pathologic conditions [1-9]. To date, none have dealt exclusively with a series of cases of a single tumor type. Very few MR images of pituitary adenomas or apparently normal pituitary glands have been presented [4, 7, 10-12]. Our study represents an evaluation of MR imaging in a consecutive series of 10 patients with pituitary adenomas, using a prototype resistive magnet MR system. Effectiveness of MR imaging was compared with that of CT.

CT is dependent for image contrast upon variations of x-ray attenuation, produced largely by variations in electron density of tissues. Further, detection and evaluation of pituitary adenomas require the use of intravenous contrast enhancement and, occasionally, intrathecal contrast methods. Proton (¹H) MR imaging exploits the interactions of static and dynamic magnetic fields, radiofrequency (RF) energy, and hydrogen nuclei, yielding information about proton density and the local physicochemical environment of protons, to the extent that this can be inferred from the relaxation time constants T1 (spin-lattice) and T2 (spin-spin). While proton density variations between different soft tissues are rather small, it has been shown that variations in the T1 and T2 relaxation times between normal and abnormal tissues are frequently very large. Suitable choices of RF pulse sequences to optimize these differences result in images with high tissue contrast (up to several hundred percent).

Subjects and Methods

Ten patients with pituitary adenomas were studied (table 1). Before MR imaging, each

Received August 10, 1983; accepted after revision October 18, 1983.

This work was supported in part by Technicare Corp., Solon, OH.

T. J. Brady is supported in part by National Cancer Institute research career development award 5 K04 CA 00848 01.

¹ Department of Radiology, Massachusetts General Hospital, Boston, MA 02114. Address reprint requests to T. J. Brady.

² Neurology, Medical and Neurological Services, Massachusetts General Hospital, Boston, MA 02114.

AJNR 5:131-137, March/April 1984

0195-6108/84:0502-0131 \$00.00

© American Roentgen Ray Society

TABLE 1: Summary of Cases with Pituitary Adenomas

| Case No. (age, gender) | Presenting Symptoms | Endocrine Abnormality | Maximum Dimensions (mm) |
|---------------------------|--|--------------------------|-------------------------------|
| 1 (45, F) | H/A, visual blurring, polyuria, polydipsia | None | ≈35 |
| 2 (20, F) | Galactorrhea and 2° amenorrhea | ↑ Prolactin (70, 86) | ≈30 |
| 3 (51, M) | H/A with recent decrease in vision, os | ↑ Prolactin (40) | ≈26 |
| 4 (13, F)* | Bifrontal H/A; family history of adenomas | None | ≈8 |
| 5 (36, F) | Galactorrhea and 2° amenorrhea | ↑ Prolactin (50, 100) | ≈12 |
| 6 (40, M) | Acromegaly for 10 years | ↑ HGH (9) | ≈14 |
| 7 (24, F) | Galactorrhea and 2° amenorrhea | ↑ Prolactin (470, 690) | ≤5† |
| 8 (22, F) | Galactorrhea and 2° amenorrhea | ↑ Prolactin (60) | ≈8 |
| 9 (28, F) | Galactorrhea and 2° amenorrhea | ↑ Prolactin (60, 100) | ≈10 |
| 10 (31, F)* | Galactorrhea and 2° amenorrhea | ↑ Prolactin (65, 88) | ≈6 |

Note.—H/A = headaches; HGH = human growth hormone. Normal prolactin is 2–15 ng/ml; normal HGH <5 ng/ml.

* No histologic confirmation.

† Partly empty sella.

adenoma had been examined by contrast-enhanced CT, with positive findings of pituitary tumor. All patients signed informed consent forms before the MR study.

MR images were acquired using a prototype system (Technicare, Solon, OH), which is based upon a resistive magnet of 0.147 T field strength (proton resonance frequency of 6.26 MHz). True three-dimensional volumetric MR data were obtained using several RF pulse sequences, including inversion recovery (IR), saturation recovery (SR), and Carr-Purcell-Meiboom-Gill spin echo (SE).

These pulse sequences have been described [13]. Briefly, the IR acquisition uses a 180°, tau, 90° type sequence with a tau value of 400 msec. In practice, the IR data are acquired concurrently with an approximate "proton density" image, which permits subsequent quantitation of T1 relaxation times [14]. The total pulse sequence repetition time is 2.2 sec. Of these two images, only the IR data are presented here.

The SR acquisition uses a 90°, tau, 90° type sequence with a tau (interpulse delay or repetition period) of 230 msec. Both IR and SR sequences use a 180° refocusing pulse, applied 16 msec after the 90° read pulse, to generate the nuclear signal (spin echo) used for image reconstruction [14]. The IR and SR techniques generate images in which the signal intensity is largely dependent upon proton density and T1 relaxation times, and to a lesser extent on T2.

The SE acquisition uses a 90°, tau, 180°, 2(tau), 180°, . . . sequence with a tau value of 30.7 msec; four 180° pulses are employed, resulting in four SE images at 61, 123, 184, and 246 msec. The sequence is repeated every 1250 msec. The SE technique generates images in which the signal intensity is determined largely by proton density and T2.

Data acquisition times are 39 min for IR, 18 min for SR, and 34 min for SE. The three-dimensional acquisition technique permits postprocessing of MR data; images can be reconstructed in any desired plane to match corresponding CT levels. The MR images presented have isotropic spatial resolutions of 1–4 mm, depending on the pulse sequence. If desired, contiguous parallel planes can be summed to yield thicker sections.

All patients had concurrent or very recent CT studies. All were intravenously contrast-enhanced studies, obtained with infusion of about 42 g of iodine over 5–7 min. All patients but one had 1.5-mm-thick transverse sections, incremented by 1 mm through the sellar and suprasellar regions, from which reformatted 1-mm-thick sagittal and coronal images were obtained. The exception was case 1, with

the largest tumor in the series, who had 5 mm transverse sections incremented by 3 mm. All the studies were obtained on a GE CT/T 8800 scanner. Intrathecal metrizamide cisternography was not used in any of the cases.

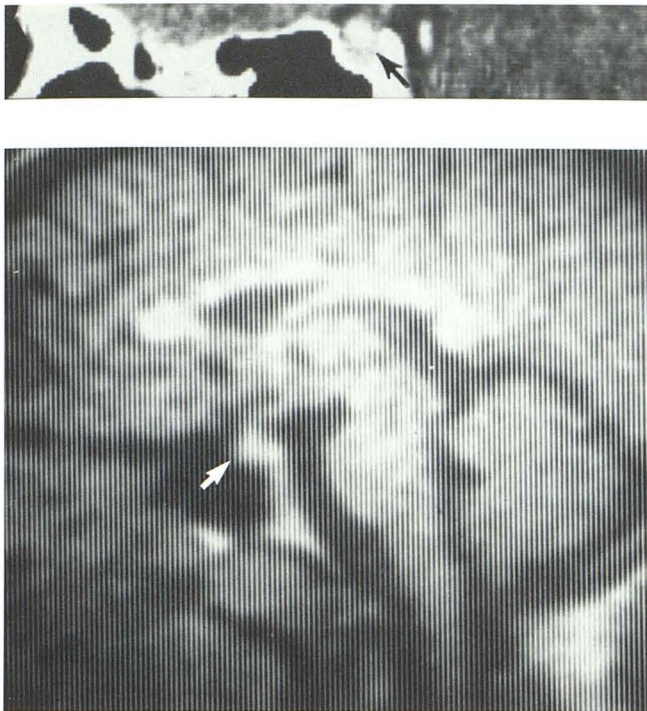
One patient had a growth hormone-secreting adenoma, seven had prolactin-secreting tumors, and two were nonfunctioning adenomas. Histologic confirmation of pituitary adenoma was obtained in eight cases. Cases 7 and 9, both with prolactin-secreting adenomas, had been treated with bromocriptine for 4 months (case 7) and 3 months (case 9) before the latest CT and the MR imaging studies (table 1).

Numerous MR images with the various pulse sequences were reconstructed to match the orientation of the CT images, and the two types of images were evaluated in detail with respect to ease of recognition of the adenoma, MR signal characteristics, CT attenuation patterns, and visibility of important regional anatomic landmarks of concern in choice of treatment.

Results

As determined from CT, the 10 tumors ranged in estimated size from less than 5-mm-diam up to 20 × 25 × 35 mm. MR imaging provided clear identification of seven of the 10 tumors. One adenoma, clearly seen on CT and estimated to be 5 × 6 × 8 mm (case 4), was detectable only by close scrutiny of the MR sections (fig. 1). The tumors of larger size (fig. 2) appeared as masses clearly larger than the normal pituitary gland, with variably altered signal intensity on IR, SR, and SE images (table 2). Only one adenoma (case 7) was not identified by CT. Four months earlier, a 13 mm prolactin-secreting adenoma had been shown by CT. At the time of the comparative study, this patient had been on bromocriptine therapy for 4 months and was now found to have a partially empty sella, within which an adenoma could not be identified either by CT or by MR imaging.

Signal intensity did not correlate with the type of adenoma. Signal intensity of the tumors was compared with that of nearby cerebral tissue (pons or cerebral white matter) and/or to the intensity of signal obtained from marrow in the clivus



B

Fig. 1.—Case 4. Nonfunctioning adenoma ≈ 8 mm diam. **A**, Nearly midsagittal contrast-enhanced CT scan reformatted from transverse sections. Markedly enhancing nodule projecting slightly into suprasellar cistern (*arrow*). **B**, Small tumor (*arrow*), with signal intensity similar to corpus callosum and lower clival marrow, projects slightly into suprasellar cistern on SR MR image. Signal intensity is slightly greater than average intensity of pons. Intensity of adenoma not distinguishable from normal gland. Just above nodule, optic chiasm, with signal less than adenoma, is contrasted against low signal of cerebrospinal fluid (CSF).

or from orbital fat. Signal intensity was termed isointense, hyperintense, or hypointense with respect to one or more of the above designated regions. Because of the variations in numeric values of T1 and T2 relaxation parameters between different imaging systems and because of certain problems in systematic corrections for these values, numeric measurements are not reported. For now, comparison of signal intensity of lesions with intensity of nearby normal anatomic structures appears to be merited.

Signal characteristics were classified as homogeneous or inhomogeneous and as high intensity (signal equal to or greater than that from clival marrow or white matter), medium intensity (signal approximately equal to that of the pons), or low intensity (signal less than that of pons and similar to that of cortical gray matter) for each type of imaging sequence. It must be borne in mind that signal intensities in any MR image depend profoundly on the exact RF pulse sequence employed, and comparisons between data obtained on different systems must be made with extreme care.

On IR, homogeneous high-intensity signal was produced by the adenomas in cases 2 and 4; none showed medium-intensity signal, and only case 9 showed low-intensity signal. Cases 3, 5, and 8 showed inhomogeneous signal on IR (mixture of high- and medium- or high- and low-signal areas).

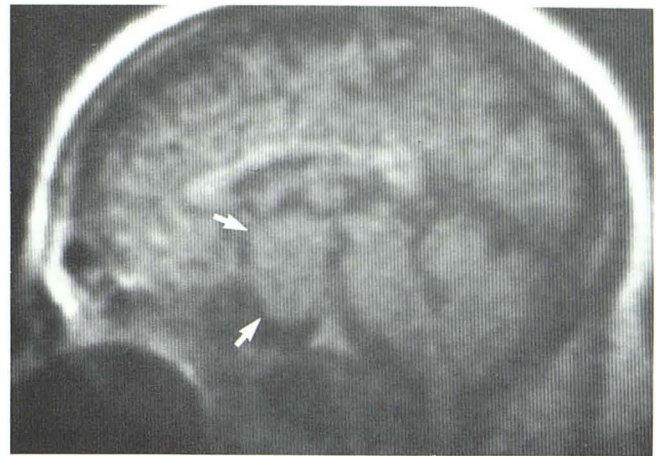


Fig. 2.—Case 1. Nonfunctioning adenoma ≈ 35 mm diam. Midsagittal section from SR image shows large mass (*arrows*) expanding sella into sphenoid sinus and projecting superiorly to compress and elevate markedly anterior third ventricle. Tumor extends into interpeduncular cistern. Truncation of clival marrow signal by tumor erosion through upper clivus into pontine cistern. Tumor signal is quite homogeneous and equals that of pons.

TABLE 2: Comparison of CT and MR Imaging in the Detection of Adenomas

| Imaging Method | No. of Adenoma Cases: | | |
|----------------|-----------------------|----------|--------------|
| | Studied | Detected | Not Detected |
| CT | 10 | 9 | 1 |
| MR: | | | |
| IR | 9 | 6 | 3 |
| SR | 9 | 7 | 2 |
| CPMG T2 | 4 | 2 | 2 |

Note.—MR = magnetic resonance; IR = inversion recovery; SR = saturation recovery; CPMG = Carr-Purcell-Meiboom-Gill sequence.

On SR, homogeneous high-intensity signal was produced by the adenomas in two cases and medium intensity by those in two others. None showed low intensity. Inhomogeneous signal on SR was noted from the adenomas in two cases, with high- and medium- or low-intensity regions. Very low-intensity signal of CSF was noted in the partly empty sella of case 7, with the solid sellar content showing low signal.

On CPMG T2 images, no adenoma showed homogeneous signal, and heterogeneous high- and medium-intensity signals were produced in two cases.

As in the case of the normal pituitary gland, on IR images, most pituitary adenomas exhibited a signal intensity less than that of the pons, markedly less than clival or dorsum sellae bone marrow, and about equal to cerebral cortex. On SR images, the tumors, like the normal gland, showed signal intensity about equal to that of the pons, cerebral white matter, and marrow. Intensity of the normal gland was difficult to obtain from a review of SE images, owing to the small size of the gland and the relatively low spatial resolution of these images on our prototype system, resulting from a lower signal-to-noise ratio than shown by more advanced systems. Two of three adenomas were seen on SE images, which showed

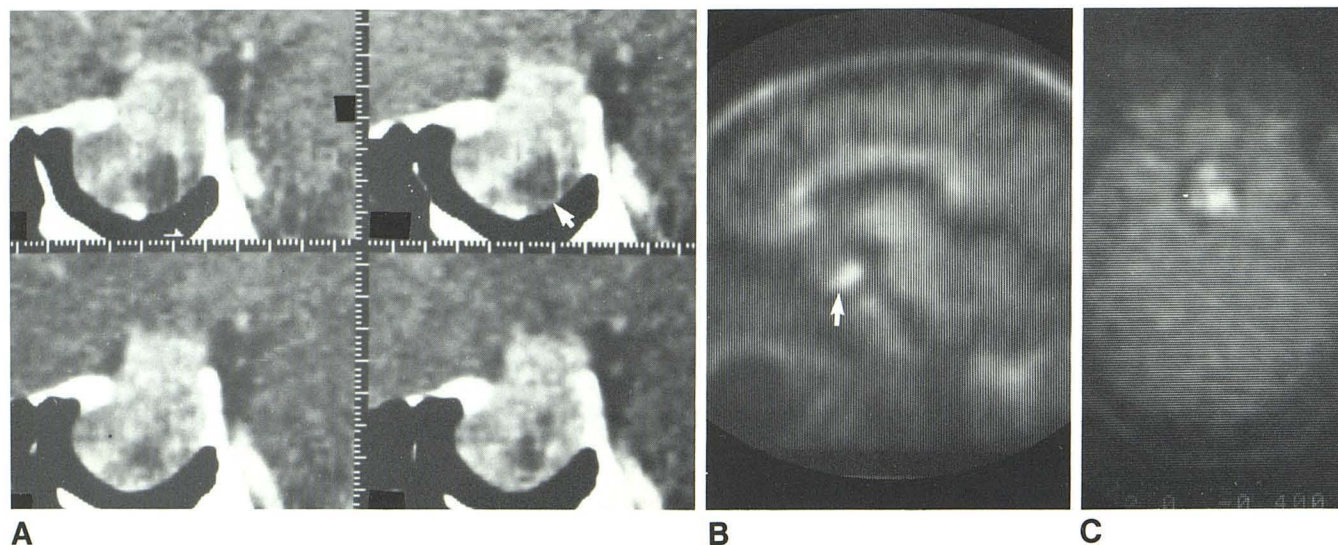


Fig. 3.—Case 3. Prolactin-secreting adenoma \approx 26 mm diam. **A**, Reformatting sagittal CT images through sella. Moderate and slightly asymmetric expansion and thinning of lamina dura from mass projecting 8 mm into suprasellar cistern. Tumor shows heterogeneous enhancement, with large and several small markedly hypodense regions, the largest of which (*arrow*) occupies right posteroinferior part of mass. **B**, IR sagittal MR image through right side of mass. Elliptical region of high signal intensity (*arrow*) similar to that of fat in posteroinferior part of tumor corresponds roughly to largest area of very low

attenuation seen on CT, indicating a short T1. The remainder of tumor has much lower signal, about equal to gray matter and greater than CSF, consistent with relatively long T1. This feature reduces contrast with suprasellar cisternal CSF, but tumor can still be identified. **D**, CPMG T2 image from third echo. Mass shows inhomogeneous signal, with areas equal in intensity to brain and several areas of high signal, consistent with prolonged T2 corresponding to region of high signal on **B**. At transsphenoidal hypophysectomy, pituitary adenoma with old hemorrhage was encountered.

TABLE 3: Comparison of CT and MR Imaging in Resolution of Perisellar Anatomy

| Imaging Method: Outcome | No. of Findings | | | | |
|-------------------------|-----------------|--------------------------------|------------------|-------------------|---------------|
| | Optic Chiasm | Anteroinferior Third Ventricle | Anterior Clinoid | Posterior Clinoid | Dorsum Sellae |
| CT: | | | | | |
| Resolved | 5/10 | 5/10 | 10/10 | 10/10 | 10/10 |
| Not resolved | 4/10 | 2/10 | 0/10 | 0/10 | 0/10 |
| Equivocal | 1/10 | 3/10 | 0/10 | 0/10 | 0/10 |
| MR: | | | | | |
| Resolved | 5/10 | 8/10 | 0/10 | 0/10 | 5/10 |
| Not resolved | 3/10 | 2/10 | 10/10 | 9/10* | 4/10* |
| Equivocal | 2/10 | 0/9 | 0/9 | 1/10 | 1/10 |

* Includes marked or complete erosion of posterior clinoids and dorsum in one case.

heterogeneous areas of isointense and hyperintense signal compared with the pons in all four echoes. The areas of hyperintense signal are consistent with regions showing a prolongation of T2 relaxation times, as seen in most other intracranial tumors and most other types of cerebral pathology, including edema.

Old hemorrhage was identified at the time of surgery and on histologic examination in cases 2 and 3. In case 3 (fig. 3), the time of hemorrhage was suggested by the history of abrupt increase in severity of headaches, in conjunction with visual deterioration about 1 month earlier. There was no evidence of increased density of fresh hemorrhage on CT, but CT appearance was compatible with an old hemorrhage or hemorrhagic infarction. The findings of a shortened T1 and lengthened T2 would certainly be compatible with a hemorrhage of this age [16].

Table 3 compares the ability of CT and MR imaging to visualize anatomic structures in the sellar and perisellar regions. The resolution of both bone landmarks and soft-tissue structures was evaluated. MR imaging was of course significantly poorer than CT in identifying osseous structures, a finding consistent with the virtual absence of mobile protons in cortical bone. The intense signal from bone marrow in the clivus served to provide an indirect indication of the posteroinferior anatomy of the sellar contents in all cases, and the truncation of the upper part of this signal corresponded to the bone erosion shown by CT in one large adenoma (case 1, fig. 2). The dorsum sellae and posterior clinoid processes may contain a small amount of marrow, identification of which is less than optimal with the spatial resolution of our imager. However, signal from marrow on these regions was identified in several cases and could be discriminated from a similarly

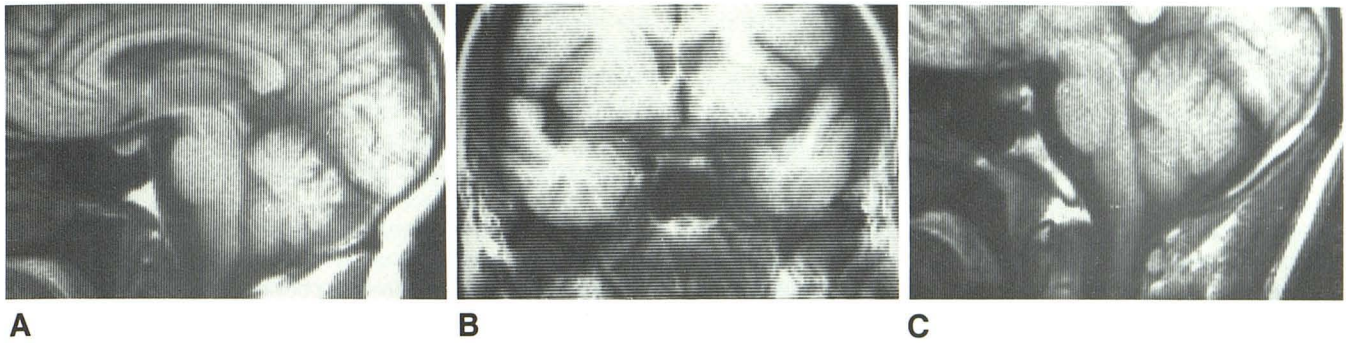


Fig. 4.—Two-dimensional sections obtained on 0.6 T MR imaging system (Technicare Corp., Solon, OH). SE sequences with 30 msec TE and 500 msec TR, using normal volunteer. Scan time was 2.2 min/section. **A**, Midsagittal section clearly demonstrates anatomy of third ventricle, optic chiasm, and pituitary gland. Mean signal intensity of gland approximates pons. Intense signal of clival bone marrow is shown clearly. **B**, Coronal section through anterior third ventricle, optic chiasm, and dorsum sellae. Intense signal below

left side of chiasm represents bone marrow in large posterior clinoid process. **C**, Midsagittal section of another normal subject, showing different configuration of clival bone marrow. Dorsum sellae is thicker and contained marrow more clearly visible than in **A**. Marrow signal of dorsum is more intense than that of pituitary gland. Anterior third ventricle, optic chiasm, and pituitary gland were clearly visible, but these window settings were chosen to accentuate marrow signal.

intense signal from the sellar contents in some instances. In no case was a signal identified from the anterior clinoid processes.

When the optic chiasm was not defined on CT and MR, a large suprasellar mass was present, obliterating detail of all of the suprasellar structures, including the hypophyseal stalk. Compression and displacement of the anterior third ventricle by tumor was visible in five of 10 CT and eight of 10 MR studies.

Discussion

Very few MR images of apparently normal pituitary glands and of pituitary adenomas have been illustrated previously and generally only large tumors have been shown. Corresponding CT images were usually not included for comparison. Signal characteristics of the tumors were only alluded to briefly [4, 7, 10–12].

Using the steady-state-free-precession (SSFP) technique, Worthington [11] illustrated a sagittal MR image showing a massive invasive chromophobe adenoma with suprasellar, transclival, and nasopharyngeal extensions. The tumor appeared heterogeneous in signal, with large areas of signal appearing similar in intensity to fat and other areas with signal only a little brighter than that of white matter. In a recent review of a large series of sellar and perisellar lesions, studied using a resistive system and SSFP techniques, Hawkes et al. [12] summarized the findings in 20 pituitary adenomas and illustrated three nonfunctioning adenomas ranging from moderate to massive size. All showed greater signal intensity than brain and all but one were homogeneous in appearance. It was concluded that MR imaging will rival CT in the assessment of pituitary disease.

Using a repeated free induction decay sequence image with a TR of 1000 msec, Steiner [7] illustrated two midsagittal MR sections showing an apparently normal pituitary gland with a homogeneous intensity slightly greater than that of the pons and appreciably brighter than clival marrow, and an IR image (400 msec interpulse interval and 1400 msec TR) showing

the gland to have a signal similar to that of gray matter and less intense than that of the pons. On the latter image, the signal from the gland was considerably less than from bone marrow. Bydder [4] presented a midsagittal SE image, with the normal-appearing pituitary gland showing a signal somewhat brighter than that of the pons and very slightly brighter than clival marrow. Bydder et al. [16] mentioned but did not illustrate one prolactinoma of unstated size, in which the T1 was said to be similar to that of two solid acoustic neuromas and three meningiomas.

The prototype MR imager used in our study has a lower signal-to-noise ratio and lower effective spatial resolution in the xy plane of transverse, sagittal, and coronal sections than certain other images of more advanced technology developed by the same and other manufacturers and in current use. However, a significant advantage over imagers operating only in a two-dimensional mode, using selective irradiation and imaging a series of contiguous sections of, for example, 7 or 13 mm in thickness, is the three-dimensional capacity of the present system, which was used in all of the adenomas studied. After three-dimensional data acquisition, any desired plane or section can be selected for reconstruction. These sections will have approximately isotropic voxels. Section orientation can be matched quite precisely with CT sections for comparison. Several images can be summated to provide thicker sections, thereby providing increased tissue contrast at the cost of additional partial-volume artifact.

Of relevance in the evaluation of MR imaging vis-à-vis CT in the study of pituitary adenomas is a reflection on the gradual evolution of the capability of CT over a period of many years, to the point that high-resolution CT has become the primary method for the diagnosis of these tumors. Currently, microadenomas of the order of 3–4 mm or greater can be recognized by these means. Intravenous contrast enhancement and good scanning techniques are required to improve the inherent tissue contrast limitations of CT. For detailed demonstration of small anatomic structures in the suprasellar area, such as the optic chiasm, hypophyseal stalk, and anterior recesses of the third ventricle, metrizamide cisternography with dilute

water-soluble contrast agents has been used to augment the relative contrast of these structures and CSF.

MR images have developed to the point that spatial resolution is quite comparable to CT. The greater contrast differential between cerebral tissues and many tumors and other lesions and CSF represents a significant advance over CT (figs. 4A and 4B). Direct coronal CT of the sella, generally agreed to offer the best orientation for evaluation of the gland, cannot always be obtained, and reformatted images from thin transverse sections suffer from increased noise. Coronal and sagittal MR images are readily obtained in two dimensions, with no degradation of quality. However, with two-dimensional methods, the slice to be imaged must be selected *before* data acquisition as in CT, but, with our three-dimensional technique, *any* slice can be displayed *after* acquisition is complete. Our results suggest that MR imaging is already quite competitive with CT in the evaluation of pituitary adenomas and that it will soon be superior to CT.

With two-dimensional imaging and appropriate pulse sequences, the cavernous sinus and internal carotid artery can be imaged separately owing to the difference in rate of blood flow between these two structures [17]. On CT, these intimate lateral relations of the pituitary gland can be discriminated among only by the use of rapid bolus intravenous contrast injection and dynamic CT imaging, a method generally not used in the evaluation of pituitary tumors.

A degree of limitation exists with respect to the absence of detectable (or distinctive) MR signal from cortical bone and calcifications. The recognition of bone erosion and altered contour is helpful in the assessment of pituitary adenomas, and the detection of various patterns of calcification is helpful in the differential diagnosis of other lesions in the region of the sella, such as craniopharyngiomas and meningiomas.

Expansion of pituitary tumors anteriorly and inferiorly is recognized readily on MR images with any pulse sequence used in our study because of the high signal contrast of the tumor versus the lack of signal from air in the pneumatized parts of the sphenoid bone. Difficulty can be anticipated in cases of largely empty sella in differentiating the low signal of CSF from the absent signal of sinus air with IR sequences. However, a suitable SE sequence should allow ready differentiation between CSF and air. Erosion by pituitary tumor into the nonpneumatized parts of the sphenoid bone, including the clivus, may be detected by means of alteration of the bright signal from marrow in these regions. However, it has been noted that the signal from pituitary adenomas and that from marrow may be similarly intense on our SR and SE pulse sequences. Unless there has been considerable hemorrhage into the tumor, IR should permit differentiation of the margin of the tumor and the regional bone marrow, since tumor signal was appreciably lower than that of marrow with this sequence.

The amount of marrow in the dorsum sellae and posterior clinoids is variable and usually quite small. When present, high spatial and contrast resolution techniques are required for its demonstration (fig. 4C). No signals were identified from the anterior clinoid processes in our cases, apparently because of a lack or paucity of contained bone marrow. Also,

the septa of the sphenoid sinus, which contain no bone marrow, were not visualized. If transphenoidal resection is contemplated, the anatomy of the sphenoid sinus and of its septa should be demonstrated. It is likely that good-quality frontal, lateral, and particular basal plain-film projections will be required to supplant MR imaging before treatment planning, if MR is to supplant CT.

Our prototype imager was capable of demonstrating the pituitary adenoma in seven of 10 cases. In one other case, a partly empty sella was identified but not the tumor, which had been reduced to an estimated size of less than 5 mm by bromocryptine therapy. In the latter case, CT was also able to identify the empty sella, but not the adenoma. The other two false-negative MR studies were in patients with adenomas estimated to be 5 × 5 × 8 mm and 6 × 6 × 6 mm, both prolactinomas. CT was able to demonstrate both of these small tumors.

Systems using higher field strength magnets with a more favorable signal-to-noise ratio than our system have better effective spatial resolution in the plane of section and should be able to resolve smaller lesions (fig. 4). Sagittal and coronal images have identified most clearly the smaller tumors, and the lack of patient manipulation required to obtain these planes represents a significant advantage of MR imaging over CT. In evaluating the superior aspect of a pituitary lesion, the high signal of the tumor on SR sequences provides a highly contrasted sharp upper margin of suprasellar protrusions of tumor against the low signal of CSF. MR imaging has proven very effective in demonstrating the optic chiasm, and the hypophyseal stalk and anterior third ventricle anatomy should be resolvable by state-of-the-art MR imagers.

ACKNOWLEDGMENTS

We thank Paul Beaulieu and Michele Haskell for assistance in data acquisition and Edith Bell for manuscript preparation.

REFERENCES

1. Buonanno FS, Pykett IL, Vielma J, et al. Proton NMR imaging of normal and abnormal brain. Experimental and clinical observations. In: Witcofski RL, Karstaedt N, Partain CL, eds. *NMR imaging. Proceedings of an International Symposium on Nuclear Magnetic Resonance Imaging*. Winston-Salem, NC: Bowman Gray School of Medicine, 1982:147-157
2. Young IR, Bailes DR, Burl M, et al. Initial clinical evaluation of a whole body nuclear magnetic resonance (NMR) tomograph. *J Comput Assist Tomogr* 1982;6:1-18
3. Crooks LE, Ortendahl DA, Kaufman L, et al. Clinical efficiency of nuclear magnetic resonance imaging. *Radiology* 1983;146:123-128
4. Bydder GM. Nuclear magnetic resonance of the brain. *Appl Radiol* 1983;12:27-33
5. Brant-Zawadzki M, Davis PL, Crooks LE, et al. NMR demonstration of cerebral abnormalities: comparison with CT. *AJNR* 1983;4:117-124, *AJR* 1983;140:847-854
6. Bydder GM, Steiner RE, Thomas DJ, Marshall J, Gilderdale DJ, Young IR. Nuclear magnetic resonance imaging of the posterior fossa: 50 cases. *Clin Radiol* 1983;34:173-188
7. Steiner RE. The Hammersmith clinical experience with nuclear

- magnetic resonance. *Clin Radiol* **1983**;34:13-23
8. Young IR, Randell CP, Kaplan PW, James A, Bydder GM, Steiner RE. Nuclear magnetic resonance (NMR) imaging in white matter disease of the brain using spin-echo sequences. *J Comput Assist Tomogr* **1983**;7:290-294
 9. McGinnis BD, Brady TJ, New PFJ, et al. Nuclear magnetic resonance (NMR) imaging of tumors in the posterior fossa. *J Comput Assist Tomogr* (in press)
 10. Hawkes RC, Holland GN, Moore WS, Worthington BS. Nuclear magnetic resonance (NMR) tomography of the brain: a preliminary clinical assessment with demonstration of pathology. *J Comput Assist Tomogr* **1980**;4:577-586
 11. Worthington BS. Clinical prospects for nuclear magnetic resonance. *Clin Radiol* **1983**;34:3-12
 12. Hawkes RC, Holland GN, Moore WS, Corston R, Kean DM, Worthington BS. The application of NMR imaging to the evaluation of pituitary and juxtaseellar tumors. *AJNR* **1983**;4:221-222
 13. Pykett IL, Buonanno FS, Brady TJ, Kistler JP. Techniques and approaches to proton NMR imaging of the head. *Comput Radiol* **1983**;7:1-17
 14. Pykett IL, Rosen BR, Buonanno FS, Brady TJ. Measurement of spin-lattice relaxation times in nuclear magnetic resonance imaging. *Phys Med Biol* (in press)
 15. Pykett IL, Buonanno FS, Brady TJ, Kistler JP. True three-dimensional nuclear magnetic resonance neuroimaging in ischemic stroke: correlation of NMR, x-ray CT and pathology. *Stroke* **1983**;14:173-177
 16. Bydder GM, Steiner RE, Young IR, et al. Clinical NMR imaging of the brain: 140 cases. *AJNR* **1982**;3:459-480
 17. Kaufman L, Crooks LE, Sheldon PE, Rowan W, Miller T. Evaluation of NMR imaging for detection and quantification of obstructions in vessels. *Invest Radiol* **1982**;17:554-560